A HIGHLY INTEGRATED LOW PRESSURE FLUID SERVO-VALVE FOR APPLICATIONS IN WEARABLE ROBOTIC SYSTEMS

Michele Folgheraiter, Mathias Jordan, Luis M. Vaca Benitez, Felix Grimminger, Steffen Schmidt
Jan Albiez and Frank Kirchner
German Research Center for Artificial Intelligence (DFKI), Robotics Innovation Center
Robert-Hooke-Strasse 5D-28359 Bremen, Germany

Keywords: Proportional Valve, Hydraulic Valve, Pneumatic Valve, Mechatronics, Pressure Control, Servo-Mechanism.

Abstract: In this paper an innovative low pressure servo-valve is presented. The device was designed with the main aim to be easily integrable into complex hydraulic/pneumatic actuation systems, and to operate at relatively low pressure ($< 50 \cdot 10^5 Pa$). Characteristics like compactness, lightweight, high bandwidth, and autonomous sensory capability, where considered during the design process in order to achieve a device that fulfills the basic requirements for a wearable robotic system. Preliminary results about the prototype performances are presented here, in particular its dynamic behavior was measured for different working conditions, and a non-linear model identified using a recursive Hammerstein-Wiener parameter adaptation algorithm.

1 INTRODUCTION

State of the art robots that are actuated with a hydraulic system are generally thought to operate with pressures greater than $200 \cdot 10^5 Pa$ (Hayward, 1994), (Jacobsen et al., 1991). This is mainly due to the fact that it is convenient to increase the force/weight ratio of the actuation system by increasing its operational pressure (Yoshinada et al., 1992). If from one side increasing the pressure brings advantages, from the other could represent a limitation. At first the hydraulic components need to be designed to resist the high forces generated by the fluid pressure; this requires therefore to employ thick and heavy materials for pipes and actuators. Secondly, the usage of high pressure could also cause a dangerous situation for the operators that are in the proximity of the robot. The safety issue is even more critical if the robot, in our case an exoskeleton, is strictly coupled with the human being (Pons, 2008). Any failure in the hydraulic system could seriously harm the user.

One of the main goal of VI-Bot project, under development at DFKI Bremen (Robotics Innovation Center), is to design an intrinsically safe, wearable arm exoskeleton for Tele-Robotics applications (Folgheraiter et al., 2008; Folgheraiter et al., 2009a; Folgheraiter et al., 2009b; Folgheraiter et al., 2009c). As requirements the haptic interface should: enable the operator to control complex robotics systems in an intuitive way, implement a multi-points haptic feedback to increase the immersion into the work scenario, be light weight and adaptable to different users, and integrate different levels of safe mechanisms. Furthermore, the kinematics architecture of the system should be designed in order to constrain as less as possible the natural arm movements and its workspace.

To achieve these goals and at the same time to reduce the complexity of the system (number of required DOF), it is necessary to keep the exoskeleton's joints near to the human arm, "ideally overlap them with the human articulations" in order to avoid parallel kinematic loops. It turns out that the necessity to have a compact, light, highly dynamic actuation system here is crucial. The advantages of using hydraulically actuators to operate the exoskeleton's joints, if directly compared with classical DC motors, are represented by their high force/weight ratio, the possibility to use the axes of the actuator as rotational/prismatic axes of the robotic system, and their back-drivability. Furthermore with a proper hydraulic supply and a precise fluid regulation, strength and high dynamic range can be achieved (Raibert et al., 2008),

Folgheraiter M., Jordan M., Benitez L., Grimminger F., Schmidt S., Albiez J. and Kirchner F. (2010).
A HIGHLY INTEGRATED LOW PRESSURE FLUID SERVO-VALVE FOR APPLICATIONS IN WEARABLE ROBOTIC SYSTEMS.
In *Proceedings of the 7th International Conference on Informatics in Control, Automation and Robotics*, pages 72-78
DOI: 10.5220/0002948700720078

(Kazerooni et al., 2006),(Kahn, 1969).

In figure 1 is shown the actual version of our haptic interface. In total there are 7 actuated joints: 5 located in the shoulder/upper-arm and 2 in the forearm. An additional passive joint allows the wrist supination-pronation. All active joints are hydraulic actuated, valves, sensors and electronics are thought to be mounted directly in proximity of the actuators, this in order to reduce the amount of cables and pipes needed. The hydraulic pump and the primary power supply are located outside the exoskeleton to avoid additional weight to the system.

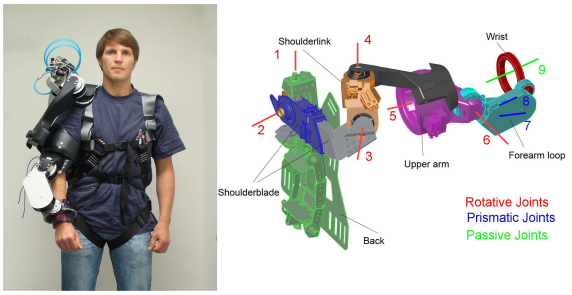

Figure 1: The arm exoskeleton equipped with 8 hydraulic rotative and linear actuators.

A central element within the hydraulic system is represented by the proportional servo-valve. On the market there are plenty of proportional (4/3) hydraulic valves, the problem is that most of them are though to work with high pressure and therefore do not fulfill our needs. According to the authors knowledge, the smallest, light weight and dynamically performing valve on the market, is currently sold by *MOOG Inc.* company (Inc., 2009). The device weights only $92g$, has an hysteresis for the flow characteristics $< 3\%$, and a 90^o phase-lag > 250Hz. Unfortunately the device is thought to work only with pressure in the range of $160 - 250 \cdot 10^5 Pa$ and it is specifically designed for Formula-1 applications.

Therefore we started to look at the pneumatic components, that generally are light and designed for low pressure (up to $10 \cdot 10^5 Pa$). We adapted them to work with liquids (oil), adding a precise actuation and proper sensory features.

This document is organized as follows: next section describes the experimental setup employed to measure the repeatability and flow-position characteristic of the valve, section 3 presents the dynamic model of the driving system, section 4 introduces a strategy to regulate position and velocity of the valve, section 5 presents a first fully integrated prototype. Finally section 6 draws the conclusions and future developments of this work.

2 EXPERIMENTAL SETUP AND TESTING

In this section the testbed developed to evaluate the performance of the servo valve and first experimental results characterising the valve are presented.
The experimental setup (figure 2) consists of the core parts of a commercial pneumatic valve (*Numatics Inc.* series Micro-Air), a stepper motor, a gear pump providing pressure supply between $0 - 30 \cdot 10^5 Pa$, a flow-meter, a pressure sensor, and an electronic board equipped with a STM32 μController.

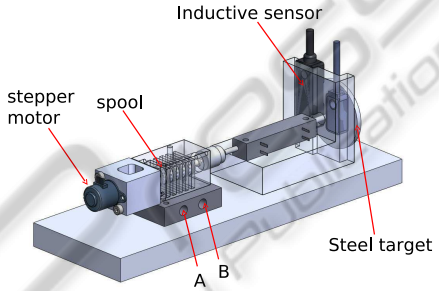

Figure 2: CAD Model of the valve testbed.

The drive system of the valve is a 3.3 V DC stepper motor from Nanotec working in fullstep mode, i.e. 18 degree/step and with an holding torque of $1.6 \cdot 10^{-3} Nm$. The rotor of the stepper motor is a lead screw, driving a cylinder and thus converting the rotational motor movement into a translation. The drive is attached to the valve spool via a permanent magnet, while the actual valve positions are determined using an inductive sensor from *Bahlluff Inc.* by tracking a steel target connected to the extended spool axis.
Control of the testbed and its components is performed by a STM32 μController (series F103VE), programmed with a special toolchain consisting of Matlab/Simulink and Rapidstm32 Blockset, Real-Time-Workshop and Keil Microvision μVision. The scheme in Figure 3 sketches the general dependencies of the testbed, were A and B are the connections of the valve to the actuator chambers, P_s and T are the pressure supply line respectively the tank lines of the gear pump, while the red lines represent the communication between the μController and the experimental setup through sensors and actors.

The two main features characterising a hydraulic valve are:

1. repeatability of the spool movement with respect to a certain input to the drive system.
2. flow through the valve with respect to spool position and the pressure drop over the valve.

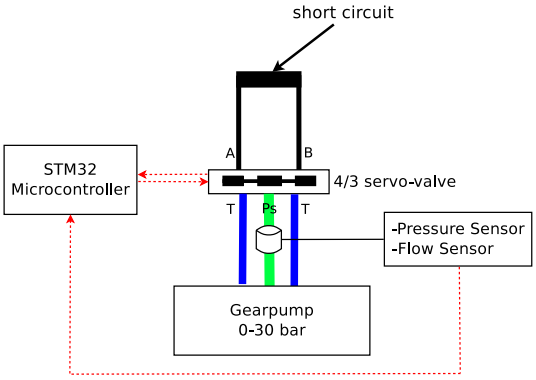

Figure 3: Scheme of experimental test setup.

Thus we focus on showing exemplary results of these two features. Position control of the fluidic valve is presented instead in section 4.

2.1 Performance of the Drive System

In the following, the ability of the valve's drive system to exactly position the spool over a long time intervall is investigated. Therefore the repeatability of valve movement is tested, by applying a special open loop control sequence. In the adjustment phase the spool is driven to the center position, while in the second phase the stepper motor is governed to move the spool 70 steps out of the zero position in both directions, which covers almost the whole working range of the developed prototype. Experiments took place under influence of pressure with $P_s = 15 \cdot 10^5 Pa$. Note that in this experiment the connectors A and B are connected in short circuit, while the speed of the motor is adjusted to its maximum of 1000 steps per second.
Figure 4 shows the open loop response of the valve prototype to the applied control sequence. The duration of the test was 20 minutes, while data was acquired for a time interval of 20 seconds every five minutes.

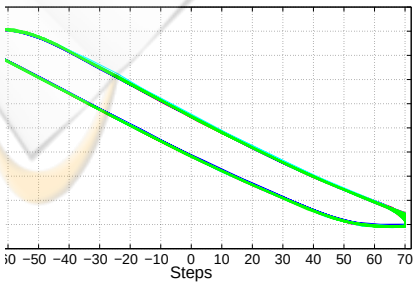

Figure 4: Position of spool while performing 70 steps out of center in both directions ($P_s = 15 \cdot 10^5 Pa$).

As we can obtain from Figure 4 the position response of the drive system to the reference signal is matching for the whole experiment. Differences for the travel of the spool, comparing the movement out of the center in both directions, might be caused by friction effects. The hysteresis is due to a backlash of approximately 10 steps (i.e. 0.1mm) between the spindle of the stepper motor and the thread of the cylinder moving the spool, when the motor changes its direction of rotation. This is due to a mechanical behavior and can only be reduced through higher precision in the manufacturing process of these two elements, or via a proper control action. Alternatively a special ball-screw could be used, which provides nearly zero backlash. Overall the valve shows remarkable repeatability for an open loop control of spool position under influence of pressure for a long time intervall.

2.2 Flow Characteristic of Valve

In this section the resulting static flow characteristic of the valve is presented.
To measure the flow for a fixed pressure drop over the valve, the connectors A and B are again linked in a short circuit, causing the valve to work against the pressure in the tank line T. A flowmeter from *Biotech* (series VZS-007-ALU) is connected to the pressure supply line providing a resolution of 900 pulses/L at a maximum flow of 5 L/min to the digital I/O of the μController. Due to the fact that flow needs a certain time to become constant, the valve is driven at a very low speed of 1 step/2s through the overall working period. Simultaneously the average flow is calculated and sampled each second.
Fig.5 shows the static flow characteristic of the hydraulic valve for a constant pressure drop of $\Delta P = 29 \cdot 10^5 Pa$.

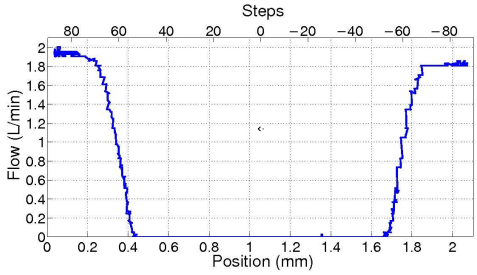

Figure 5: Flow-characteristic of the valve with respect to the spool position ($\Delta P = 29 \cdot 10^5 Pa$).

From Figure 5 we can determine that the valve has a large deadband of approximatively 1.25 mm (be-

tween 0.45 mm and 1.7 mm) where it is completely closed. This is caused by the inner structure of the valve, which is adapted from a pneumatic solenoid valve and can neither be influenced nor changed at the moment. Therefore this deadband has to be taken into account in the position control structure presented in section 4.
Having a closer look at the slopes of the flow characteristic, an area of about $0.2mm$ can be attested, where flow regulation should be possible. Driving the spool to the extremes causes flow saturation ($U_a \leq 0.2mm$ and $1.9mm \leq U_a$), thus the overall working range of the valve prototype can be defined to

$$0.15mm \leq U_a \leq 1.95mm,$$

whereas the amplitude of the flow depends on the pressure drop over the valve.
The exemplary results shown in this section certify a good repeatability to the drive system of the developed prototype. Furthermore the static flow characteristic promises a possible flow regulation within the defined working range.

3 DYNAMIC MODEL

In this section a non-linear dynamic model that takes into account the electromechanical behavior of the stepper motor, the mechanical behavior of the spool and the static/dynamic effects of the frictions present within the system, was identified using a recursive Hammerstein-Wiener Parameter Adaptation Algorithm (PAA). The linear part of the model can be considered as an ARX structure, well known from the Recursive Least Squares(RLS) Algorithm described in (I. Landau, 2006). On the other hand, the input and output non-linearities with order nl of a Hammerstein-Wiener model have the form

$$\eta(u) = \sum_{k=2}^{n_l} \beta_k u^k \tag{1}$$

$$\eta(y_{lin}) = \sum_{k=2}^{n_l} \gamma_k y_{lin}^k \tag{2}$$

with y_{lin} as the output of the linear part.

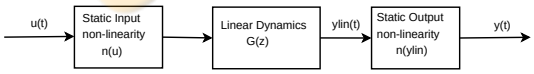

(3)

Figure 6: Block diagram of a non-linear Hammerstein-Wiener model.

Using the equation for a Hammerstein-Wiener models output (Guo, 2004), the structure of the PAA becomes, with u(t) and y(t) being the real input and output signals of the system:

$$\hat{\theta}(t+1) = \theta(t) + F(t+1)\phi(t)\varepsilon^0(t+1) \tag{4}$$

with the Adaptation Gain

$$F(t+1) = F(t) - \frac{F(t)\phi(t)\phi(t)^T F(t)}{1+\phi(t)^T F(t)\phi(t)} \tag{5}$$

and the Prediction Error

$$\varepsilon^0(t+1) = y(t+1) - \hat{\theta}(t)^T \phi(t). \tag{6}$$

$\hat{\theta}$ is the vector of computed parameters, with

$$\hat{\theta}(t)^T = [\hat{a}(t)^T, \hat{b}(t)^T, \hat{\beta}(t)^T, \hat{\gamma}(t)^T], \tag{7}$$

where $\hat{a}(t)^T = [\hat{a}_1(t)...\hat{a}_{na}(t)]$ are the parameters of polynomial A with order na, $\hat{b}(t)^T = [\hat{b}_1(t)...\hat{b}_{nb}(t)]$ the parameters of polynomial B with order nb, $\hat{\beta}(t)^T = [\hat{\beta}_1(t)...\hat{\beta}_{nl}(t)]$ the parameters of the input non-linearity with order nl, $\hat{\gamma}(t)^T = [\hat{\gamma}_1(t)...\hat{\gamma}_{nl}(t)]$ the parameters of the output non-linearity with order nl.

Furthermore $\phi(t)$ is the Predictor Regressor Vector

$$\phi(t)^T = [-y(t), u(t), u(t)^2, ..., u(t)^{nl}, y_{lin}(t)^2, ..., y_{lin}(t)^{nl}]. \tag{8}$$

The output of the linear part y_{lin} cannot be measured, nevertheless it can be calculated by multiplying the parts of the predictor and the parameters vector corresponding to the linear model:

$$y_{lin}(t+1) = \hat{\theta}[1 : na+nb+nl](t)\phi[1 : na+nb+nl] \tag{9}$$

Finally the model output $\hat{y}$ is computed

$$\hat{y}(t+1) = \hat{\theta}(t+1)^T \phi(t) \tag{10}$$

The measured signals used for identification are the current absorbed by the stepper motor i_M as input signal, and position of the valvespool x_S in terms of mm as output. In order to characterize the dynamic behavior of the valve we only considered the range of spool positions where the flow can be effectively regulated. As a first step the data was filtered using a bandpass filter allowing frequencies between $0Hz$ and $60Hz$, which does not affect the dynamic range of the model. Different models were identified starting from distinct initial values for the parameter vector, the best data fitting reached an average of 87.49%. The output of the obtained model can be seen in Figure 7,

whereas the transfer function of the linear dynamic part is given by:

$$G(z) = \frac{-0.1675z - 0.1039}{z^3 - 0.8512z^2 - 0.1351z - 0.03855} \quad (11)$$

with the sample time 0.01s. The Bode diagram of G(z) is shown in Figure 8. Finally the static input non-linearity of the model was identified to:

$$\eta(u) = 0.59831 * u^2 - 0.00047669 * u^3, \quad (12)$$

while the static output non-linearity of the model is given by:

$$\eta(y_{lin}) = 0.030651 * y_{lin}^2 - 0.042948 * y_{lin}^3 \quad (13)$$

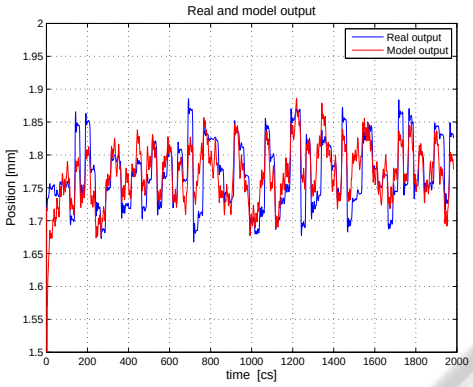

Figure 7: Comparison of the real and the model output.

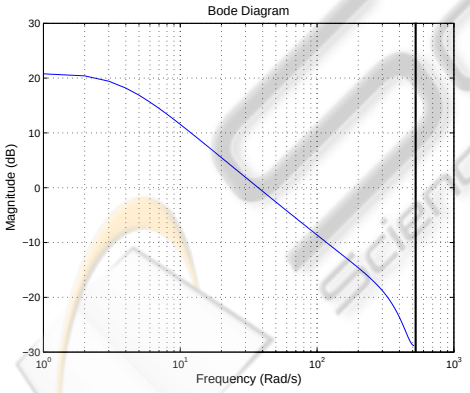

Figure 8: Magnitude Bode Plot of the linear transfer function.

4 VALVE CONTROL

This section introduces a first approach to control the developed fluidic valve.
Regarding the experiments shown in section 2, up to now all movements of the spool have been performed in open loop, i.e. no feedback of the spool position was used. To facilitate precise position control of the valve at a high bandwidth, the drive system is to be controlled in closed loop, using the feedback of the inductive sensor to track the desired trajectories given by the μController. Therefore classical PID-control in combination with a discretisation of stepper motor motion is applied.
A basic requirement for position control is the ability of the drive system to run at different speeds. Due to the fact that the stepper motor is somehow a digital drive, which can only have the states *run* or *stop*, a discretising function is introduced to the control loop. The idea is to vary the number of samples passing between two step commands by defining a variable delay factor τ_d, which causes a step command only every $\tau_d * T_s$, with T_s as basic sampling time of the system. Thus an increase of τ_d results in a slower motion of the valve spool, because less steps are performed by the drive system in a fixed time interval.
The value of τ_d is set by the control action u of the PID-controller, tracking the desired spool position p_d, as follows

$$\tau_d = \begin{matrix} 15 - |u| \cdot 500 & , u \leq 0.03 \\ 1 & , u > 0.03 \end{matrix} \quad (14)$$

Figure 9 shows the resulting scheme of the closed loop control.

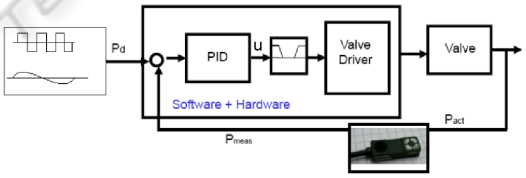

Figure 9: Scheme of discretised closed loop valve control.

Whereas p_{meas} represents the measured and p_d the desired spool position. The discretising function can be found between the PID-controller and the valve driver.
To reject noise from the position measurement, a moving average low-pass filter is realised via software in the μController. The following Figure 10 shows the modulation of the valve speed through the discretising function.

To verify the functionality of the control startegy, the valve is governed to execute a velocity sweep. Starting from $\tau_d = 100$ the delay factor is decreased by an amount of five every 5 ms until the maximum speed at $\tau_d = 1$ is reached. After changing the direction of movement τ_d is reset to its starting value. It is obvious that the speed of the valve is increased

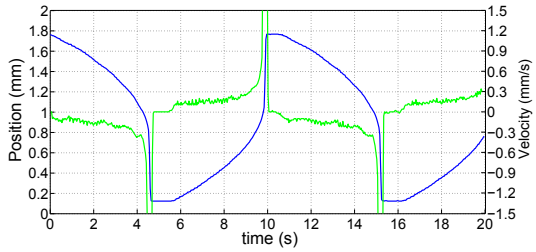

Figure 10: Speed modulated fluidic valve, blue: valve position, green: velocity.

while the delay factor decreases and vice versa.
To test the overall performances of the developed control scheme, sinusoidals with different frequencies and step-like reference trajectories were supplied. The PID's parameters have been determined through classical Ziegler-Nichols method, whereas the critical controller gain and the critical oscillation period were respectively identified as $K_{p,crit} = 0.58$ and $T_{crit} = 0.032\,s$. These results in the following controller gains

$$K_p = 0.35\,,\, K_i = 0.02\,,\, K_d = 0.004\,.$$

Figure 11 exemplary presents the tracking results of the position control loop for step-like reference signals.

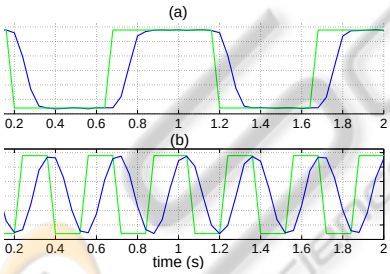

Figure 11: Step-like reference tracking at (a) f=1Hz, (b) f=3Hz, where the green line represents the reference.

As we can obtain from the figure, the controller tracks step-like signals without overshoot up to an actual maximum frequency of f=3Hz. Due to the fact that this test is performed in the maximum working range, a better dynamic response can be expected for smaller movements.
Finally Table 1 sums up the characteristic values for a sinusoidal reference tracking, where f is the frequency of the reference, e_{pmax} the maximum error in position and φ the phase shift between the two signals.

Table 1: Chracteristic values for sinusoidal reference tracking.

f in [Hz]	e_{pmax} in [V]	φ in [deg]
0.5	0.028	0.81
1	0.032	1.8
3	0.11	3.24

5 THE VALVE PROTOTYPE

After the choice of the proper hardware and electronic components, a new valve was designed and realized (figure 12) using rapid prototyping technique. The final device has a volume of LxWxH=(60mm)x(20mm)x(40mm), and the version with aluminum parts will weight approximately 80g including one position and two pressure sensors, an amplifier board, the stepper motor, and the electrical/hydraulic connectors.

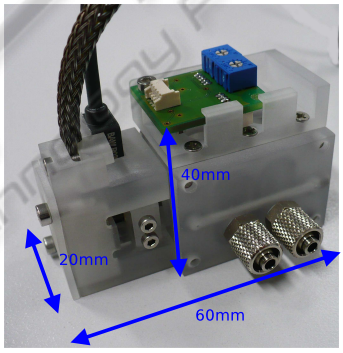

Figure 12: Valve developed using rapid prototyping technique.

In this first prototype the PWM motor driver and the control logic are located in a separated device, nevertheless future versions may also include these components on-board. This will reduce the amount of required cables to only a single power and a data line (e.g. a CAN-BUS). Compared with other state of the art hydraulic valves (Inc., 2009), the one here presented is designed to work with relatively low pressures both for hydraulic and pneumatics purposes, it is extremely compact and light-weight, furthermore it integrates two pressure sensors that are directly connected to the two output lines A and B (see schema in figure 2). This allows a fine tuning of the pressure inside the two actuator chambers, and therefore enables a precise control of the generated torque.

6 CONCLUSIONS AND FUTURE DEVELOPMENTS

In this paper a new fluid servo-valve specifically designed for wearable robotic systems is presented. The work is motivated by the fact that, according to the authors knowledge, no commercial valve exists for precise low pressure hydraulic actuators control. As general requirements, compactness, light-weight, and high dynamics were considered during the design process. A first series of experiments have been performed to test repeatability, flow-position characteristics and dynamic response. A model of the drive system of the servo-valve was identified using a recursive Hammerstein-Wiener parameter adaptation algorithm. The combination of a linear and dynamic part with a non linear static component let to reach a fit of 87%. Finally to test the overall functionality of the valve and to measure its step response characteristics, a proper control algorithm was implemented that allows to regulate the position and the velocity of the valve's spool.

Further work have to be dedicated in order to identify the overall model that will explicitly define the position-flow-pressure relationship. The backlash and deadband problems need to be properly addressed. In particular the employment of a ball-screw for the roto-translation mechanism of the valve, instead of a normal lead screw , will improve the precision in controlling the position. Furthermore, with a customized design of the spool, will be possible to decrease the switching time between the two opening positions, and therefore to improve the dynamic behavior of the servo-valve.

ACKNOWLEDGEMENTS

The work presented in this paper was done within the VI-Bot project, funded by the German Ministry of Science (BMBF), [grant number 01IW07003].

REFERENCES

Folgheraiter, M., Bongardt, B., Albiez, J., and Kirchner, F. (2008). A bio-inspired haptic interface for telerobotics applications. In *IEEE International Conference on Robotics and Biomemetics (ROBIO-2008)*, Thailand, Bangkok.

Folgheraiter, M., Bongardt, B., Albiez, J., and Kirchner, F. (2009a). Design of a bio-inspired wearable exoskeleton for applications in robotics. In *International Joint Conference on Biomedical Engineering Systems and Technologies (BIOSTEC-2009)*, Portugal, Porto.

Folgheraiter, M., de Gea, J., Bongardt, B., Albiez, J., and Kirchner, F. (2009b). Bio-inspired control of an arm exoskeleton joint with active-compliant actuation system. *Applied Bionics and Biomechanics*, 6(2):193–204.

Folgheraiter, M., Schmidt, B. B. S., de Gea Fernandéz, Albiez, and Kirchner, F. (2009c). Design of an arm exoskeleton using an hybrid motion-capture and model-based technique. In *IEEE International Conference on Robotics and Automation. IEEE International Conference on Robotics and Automation (ICRA-2009), May 12-17, Kobe, Japan*.

Guo, F. (2004). *A New Identification Method for Wiener and Hammerstein System*. PhD thesis, Karlsruhe University.

Hayward, V. (1994). *Experimental Robotics III, Design of a hydraulic robot shoulder based on a combinatorial mechanism*, volume 200. Springer Berlin / Heidelberg.

I. Landau, G. Z. (2006). *Digital Control Systems*. Springer.

Inc., M. (2009). Sub miniature servovalve e024. Technical report, http://www.moog.com/.

Jacobsen, S. C., Smith, F. M., Backman, D. K., and Iversen, E. K. (1991). High performance, high dexterity, force reflective teleoperator ii. In *Proc. ANS Topical Meeting on Robotics and Remote Systems*.

Kahn, M. (1969). *Optimal Control of a Hydraulic Arm*. PhD thesis, Stanford University M.E Dept.

Kazerooni, H., Steger, R., and Huang, L. (2006). Hybrid control of the berkeley lower extremity exoskeleton (bleex). *The International Journal of Robotics Research*, 25(5-6):561–573.

Pons, J. L., editor (2008). *Wereable Robots: Biomechatronixs Exoskeletons*. Wiley.

Raibert, M., Blankespoor, K., Nelso, G., Playter, R., and the BigDog Team (2008). Bigdog, the rough-terrain quaduped robot. Technical report, Waltham, MA 02451 USA.

Yoshinada, H., Yamazaki, T., Suwa, T., and Naruse, T. (1992). Design and control of a manipulator system driven by seawater hydraulic actuator. In *Second Int. Symposium on Measurement and Control in Robotics (ISMCR)*, pages 359–364.